Study of myocardial cell inhomogeneity of the human heart: Simulation and validation using polarized light imaging

Paul Audain Desrosiers[a)]
CREATIS, CNRS UMR 5220, INSERM U1206, University of Lyon, INSA Lyon, Lyon 69621, France and TIMC-IMAG, CNRS UMR 5525, University of Grenoble Alps, Grenoble 38706, France

Gabrielle Michalowicz and Pierre-Simon Jouk
TIMC-IMAG, CNRS UMR 5525, University of Grenoble Alps, Grenoble 38043, France and Genetics Department, CHU Grenoble-Alps, CS 10217 Grenoble, Grenoble Cedex 9 38043, France

Yves Usson
TIMC-IMAG, CNRS UMR 5525, University of Grenoble Alps, Grenoble 38706, France

Yuemin Zhu
CREATIS, CNRS UMR 5220, INSERM U1206, University of Lyon, INSA Lyon, Lyon 69621, France

(Received 1 October 2015; revised 18 March 2016; accepted for publication 21 March 2016; published 7 April 2016)

Purpose: The arrangement or architecture of myocardial cells plays a fundamental role in the heart's function and its change was shown to be directly linked to heart diseases. Inhomogeneity level is an important index of myocardial cell arrangements in the human heart. The authors propose to investigate the inhomogeneity level of myocardial cells using polarized light imaging simulations and experiments.
Methods: The idea is based on the fact that the myosin filaments in myocardial cells have the same properties as those of a uniaxial birefringent crystal. The method then consists in modeling the myosin filaments of myocardial cells as uniaxial birefringent crystal, simulating the behavior of the latter by means of the Mueller matrix, and measuring the final intensity of polarized light and consequently the inhomogeneity level of myocardial cells in each voxel through the use of crossed polarizers. The method was evaluated on both simulated and real tissues and under various myocardial cell configurations including parallel cells, crossed cells, and cells with random orientations.
Results: When myocardial cells run perfectly parallel to each other, all the polarized light was blocked by those parallel myocardial cells, and a high homogeneity level was observed. However, if myocardial cells were not parallel to each other, some leakage of the polarized light was observed, thus causing the decrease of the polarized light amplitude and homogeneity level. The greater the crossing angle between myocardial cells, the smaller the amplitude of the polarized light and the greater the inhomogeneity level. For two populations of myocardial cell crossing at an angle, the resulting azimuth angle of the voxel was the bisector of this angle. Moreover, the value of the inhomogeneity level began to decrease from a nonzero value when the voxel was not totally homogeneous, containing for example cell crossing.
Conclusions: The proposed method enables the physical information of myocardial tissues to be estimated and the inhomogeneity level of a volume or voxel to be quantified, which opens new ways to study the microstructures of the human myocardium and helps understanding how heart diseases modify myocardial cells and change their mechanical properties. [http://dx.doi.org/10.1118/1.4945272]

Key words: myocardial cells, fiber architecture, human heart, homogeneity level, polarized light imaging

1. INTRODUCTION

The myocardium is a muscle made of three-dimensional (3-D) network of myocardial cells connected by anastomoses;[1] the network or arrangement pattern is highly structured and is described as a multilayered organization where each layer of myocardial cells has a preferred orientation.[2] This architecture of myocardial cells or myocardial fibers (by abuse of language) plays a fundamental role in the heart's function and its change was shown to be directly linked to heart diseases.

Many methods for studying the fiber architecture of the myocardium have been reported in the literature. We can cite three main approaches: histological technique,[1–5] diffusion magnetic resonance imaging (dMRI),[6–9] and polarized light imaging (PLI).[10–24] Especially, PLI was used to analyze the healing after myocardial infarction,[10] establish the map of myofiber patterns in the second trimester fetal human heart,[11] study the fiber architecture of the ventricle during fetal and neonatal life,[12] analyze collagen network,[13] investigate the topography of myocardial cells during embryonic and fetal life

development,[14] and characterize the myocardium including healthy, infarcted, and stem cell regeneration tissues.[15] Owing to its high spatial resolution ($0.1\times0.1\times0.5$ mm for an entire adult human heart) and 3-D nature, PLI is today considered a gold-standard technique allowing to provide the ground-truth of the myocardial cell architecture of *ex vivo* human hearts.

However, almost all existing work was basically focused on the study of the orientation of myocardial cells. To describe more quantitatively myocardial cell arrangement patterns, the notion of homogeneity (or inhomogeneity) level of myocardial cells was introduced by Usson *et al.*;[16] the work consisted in physically measuring, by means of a confocal microscopy, the homogeneity level of myocardial cells, in a very small two-dimensional region of the myocardium.

In this paper, we propose to investigate such notion of inhomogeneity level of myocardial cells, initially introduced in the case of confocal microscopy, using PLI. The idea is based on the fact that the myosin filaments in myocardial cells have the same properties as a uniaxial birefringent crystal,[12,17] and that myocardial cells can then be modeled as uniaxial birefringent crystals. Thus, we simulate the behavior of a uniaxial birefringent crystal by means of the Mueller matrix, and measure the final intensity of polarized light and consequently the inhomogeneity level of myocardial cells in each volume or voxel (in what follows the term volume also designates the voxel) through the use of crossed polarizers.

2. MATERIALS AND METHODS

2.A. Design of the experimental PLI system

To study the inhomogeneity level of myocardial cells in each voxel under polarized light, an experimental PLI system was designed and constructed as illustrated in Fig. 1.

The unpolarized light source was made of 144 white LEDS. The depolarizer ensures that the light is unpolarized. The two crossed polarizers were driven together by two motors step by step (0°–360°). A linear camera Pulnix TM-6EX was mounted on the top of the second polarizer to record the images. The PLI was totally controlled and monitored by the software we have developed in c/c++ under Linux OS (see Sec. 3.D).

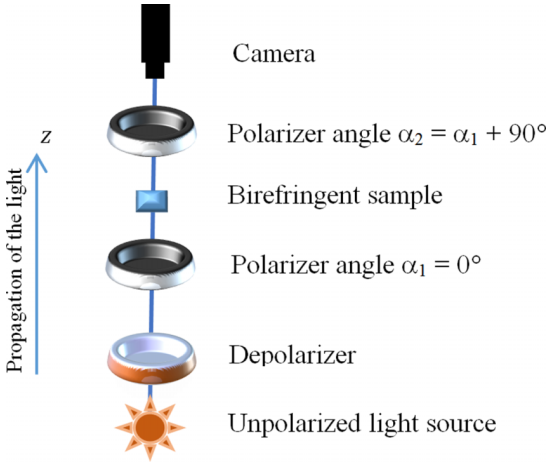

FIG. 1. Scheme of the PLI system used for the simulation.

Light is an electromagnetic wave having two main components: the magnetic field vector and electric field vector; these vectors are orthogonal to each other. With a polarized light, the electric field vector vibrates in one fixed direction, perpendicularly to the direction along which the light propagates. The light beam is composed of waves whose vibration axes are randomly distributed. The polarizer is an optical element which selects a specific direction of vibration of the light. When the selection axes of the two polarizers are perpendicular to each other, without any birefringent sample between them, the light is blocked and its intensity is down to zero. However, if a birefringent sample is present and rotated between the two crossed polarizers, it interferes with the light vibrating axes and some light is transmitted across the second polarizer. When the selection axes of two polarizers are parallel to each other, all the polarized light is transmitted.

2.B. Simulation of PLI

The amount of transmitted light is a function of the birefringence of the sample, and this birefringence is a function of physicochemical characteristics of the sample and the orientation of the latter with respect to the incident light. In the human heart, collagen birefringence is a second type of birefringence;[12] it is highly variable, depending on the kind of collagen under examination and must be neutralized as much as possible. This is achieved by embedding the sample in methyl methacrylate (MMA)[12,14,17] that has the same refraction index as collagen. Thus, the myocardium embedded in MMA behaves like a quasicrystal and quantitative polarized light can be measured to characterize its properties. In order to collect the myosin birefringence ($\Delta_{max} = 10^{-4}$) signal alone, we cancel out all the collagen structure birefringences.[12]

When a polarized beam crosses a uniaxial birefringent sample, it is divided into two rays (ordinary and extraordinary). The electrical fields of the two rays vibrate perpendicular to each other with a phase difference which depends on the structural properties of the sample.[20,21] The birefringence $\Delta_n = (n_e - n_o)$ of the uniaxial sample was measured as the difference of refraction indexes of the ordinary ray n_o and the extraordinary ray n_e.[21] In order to simulate the optical elements of the above depicted PLI system and also to take account of the depolarization state of the polarized light of the simulated or real tissue, we use the Mueller matrix which was initially proposed by Hans Mueller for representing any optical element by a 4×4 matrix.[22] The Mueller matrix of the output of the PLI system can then be expressed as

$$M_O = M_{P(\alpha_2)} \times M_{s(2\theta,\varphi(\Phi))} \times M_{P(\alpha_1)} \times M_D, \quad (1)$$

where

- M_p: the Mueller matrix of the two polarizers.
- M_s: the Mueller matrix of the uniaxial birefringent sample.
- M_D: the Mueller matrix of the depolarizer.
- α_1, α_2: the rotation angle of the first and the second polarizers, respectively.

— Φ, θ: the elevation angle and the azimuth angle of the birefringent sample, respectively.
— $\varphi(\Phi)$: the phase shift of the birefringent sample with respect to the elevation angle Φ.

The matrices M_p, M_s, and M_D are given by Desrosiers *et al.*[17] The first element $m_0(0,0)$ of the output Mueller matrix M_O gives the final amplitude of the polarized light. Assume that the input light is completely depolarized (M_D is a constant matrix). When there is no object, M_s is an identity matrix, and, as a result, M_O will be a zero matrix and the amplitude of the polarized light is zero.

Thus, from Eq. (1), the first element $m_0(0,0)$ of M_O can be derived

$$m_0(0,0) = ((1-\cos\varphi) - (1-\cos\varphi)\cos(-4\theta+\pi+4\alpha))/8. \quad (2)$$

Since the azimuth angle θ is fixed in the experiment, (2) depends only on α and φ. The first element $m_0(0,0)$ can further be simplified as

$$m_0(0,0)_\alpha = u\left(\cos\left(4\left(-\theta+\frac{\pi}{4}+\alpha\right)-1\right)\right). \quad (3)$$

Or more simply

$$m_0(0,0)_\alpha = u\cos^2\left(2(\alpha+\frac{\pi}{4}-\theta)\right) \quad (4)$$

with $u = (1-\cos\varphi)/8$.

If we fix φ, then we can deduce from the formulae Eqs. (7) and (8) given by Desrosiers *et al.*,[17]

$$\frac{u}{u_{\max}} = \cos^4(\Phi), \quad (5)$$

where $u_{\max}$ depends on the elevation angle of the volume. By writing

$$u_{\max}\cos^4(\Phi) = B, \quad (6)$$

with B representing the maximum amplitude of the polarized light, the above expression can be written as

$$m_0(0,0)_\alpha = B\cos^2\left(2(\alpha+\frac{\pi}{4}-\theta)\right). \quad (7)$$

If $\Phi = 0$ in Eq. (5), we have $u = u_{\max}$, which means that, at this particular value of Φ, the amplitude of polarized light is maximum.

When a birefringent sample is present (i.e., M_s contains non-zero elements), its optical axis interferes with the light vibrating axes of the two polarizers $M_{(P1)}$ and $M_{(P2)}$ and some light is transmitted across the second polarizer. For the given two crossed polarizers $M_{P1(\alpha_1=0°)}$ and $M_{P2(\alpha_2=90°)}$, the variation of the polarized light only depends on the physical structure of the birefringent sample under investigation. When the sample presents parallel structures, the amplitude of the polarized light will increase. When the sample has crossing structure, the amplitude of the polarized light will decrease. The amplitude of the polarized light therefore reflects the spatial arrangement of myocardial cells in the sample. This led us to introduce the notion of inhomogeneity level of myocardial cells by adding an offset A to the first element $m_0(0,0)$ of the output Mueller matrix M_O,

$$y(\alpha) = A + m_0(0,0)_\alpha = A + B\cos^2\left(2(\alpha+\frac{\pi}{4}-\theta)\right), \quad (8)$$

where $y(\alpha)$ represents the final amplitude of the polarized light received by the camera.

Note that the additive offset A in Eq. (8) is based on the assumption that the myosin filament has the same property as a uniaxial birefringent crystal. The proposed model can then be applied to any birefringent biological tissues, provided the tissues have the same property as a birefringent uniaxial crystal. Such additive model however could not hold when the crystal under investigation is biaxial or triaxial.

The value of A determines the inhomogeneity level of the sample volume at a voxel. If A equals zero, the inhomogeneity level is zero, indicating that the volume is totally homogeneous. If the offset A increases, the inhomogeneity level will increase. To evaluate the measurement of inhomogeneity level of myocardial cells in the human heart, different myocardial cell configurations in a voxel (tissue volume) were simulated. The spatial configuration was modeled as a mixture of small uniaxial birefringent elements. The tissue corresponds to a volume of $100 \times 100 \times 500$ μm^3 which is divided into 25 elements. Each of the elements is formed of 25 cells with 20 μm in diameter and 100 μm in length. For each element, we set its local 3D orientation (azimuth and elevation angles) in a manner that various conditions are experienced: homogeneous volume (all myocardial cells are parallel) and heterogeneous volume (myocardial cells have different orientations with solid angle dispersion). In practical experiments, the inhomogeneity level of myocardial cells in a voxel depends on the standard deviation σ in orientations of the myocardial cells in the volume. The orientation is defined by two angles: azimuth angle and elevation angle. The azimuth angle θ is the angle between the west-east axis of the stage (x-axis) and the projection of the uniaxial sample orientation on the stage plane, and the

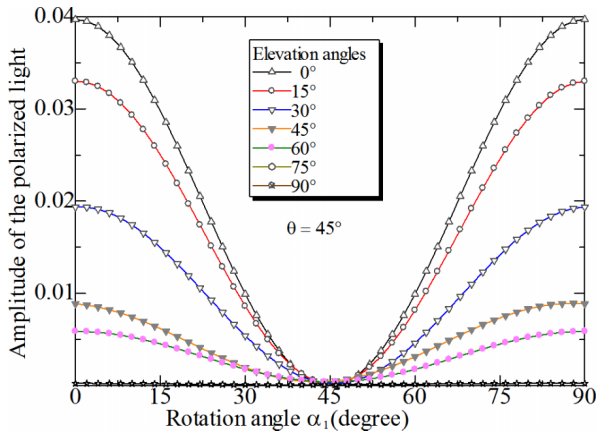

FIG. 2. Variation of the light amplitude as a function of rotation angles of the two crossed polarizers for a uniaxial birefringent sample (homogeneous volume with a solid dispersion angle of zero). The azimuth angle of myocardial cells was set to a fixed value of 45°, while the elevation angle Φ varied from 0° to 90°. Note that the amplitude of 1.0 corresponds to the initial amplitude of the depolarized light source.

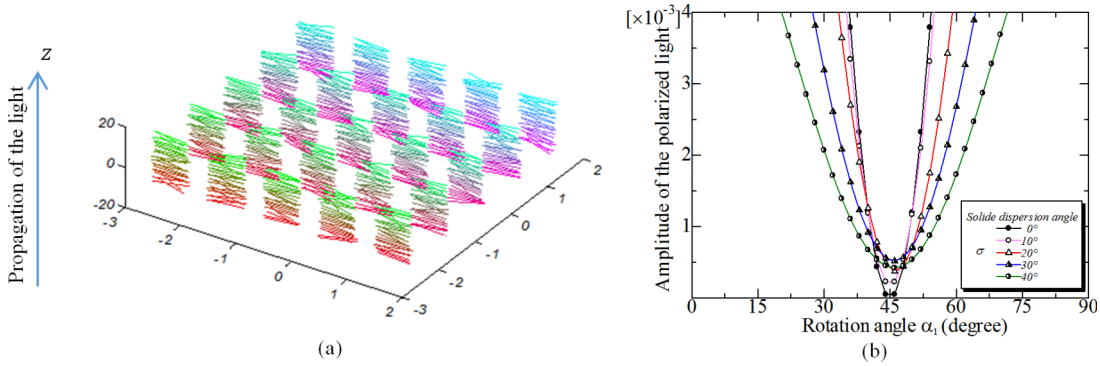

FIG. 3. (a) Simulated heterogeneous volume with a solid dispersion angle of 15°. Each cell is represented by a different color. (b) Variation of the light amplitude of a heterogeneous volume as a function of the rotation angle of the two crossed polarizers. Each curve corresponds to a given solid dispersion angle that varies from 0° to 40°.

elevation angle Φ corresponds to the obliquity of the uniaxial sample with respect to the plane of the section.

To estimate the inhomogeneity level of myocardial cells in a voxel, we used two crossed polarizers that rotate at the same time. The first polarizer of angle α_1 was rotated from 0° to 90° and the second polarizer of angle α_2 was rotated such that $\alpha_2 = \alpha_1 + 90°$ (thus forming two crossed polarizers). When the selection axis of the first polarizer is parallel to the optical axis of the sample, the final amplitude of the polarized light will drop to zero.[17] Thus, the selection axis of the first polarizer can help us to define the orientation of birefringent samples (or birefringent crystals) and myocardial cells in real tissues like those we used in Sec. 3.D. All the simulations were performed under GNU/Octave on Linux OS.

3. RESULTS AND DISCUSSIONS

3.A. Homogeneous volume with parallel myocardial cells

The simulated homogeneous volume is composed of perfectly parallel myocardial cells. The azimuth angle θ of the volume was set at 45°, and the elevation angle Φ was varied from 0° to 90°. For each fixed angle pair (azimuth angle, elevation angle), we vary the rotation angle α_1, and the output polarized light is calculated using Eq. (1). As observed in Fig. 2, for each fixed elevation angle, the amplitude of the output polarized light varies with rotation angle. At the rotation angle of 45°, all the curves drop to zero, which means that at this rotation angle, there is no light coming out of the second polarizer. This is due to the fact that, at this rotation angle, the selection axis of the first polarizer is parallel to the optical axis of the volume. Since the output polarized light is zero at this rotation angle, we can derive from Eq. (8) that the inhomogeneity level A is zero. This simulation result conforms to that obtained with the physical optical bench.[16,17,23] These results also imply that, at the rotation angle of 45°, the azimuth angle θ is independent of the PLI system.

3.B. Heterogeneous volume with solid angle dispersion

We now simulate a heterogeneous volume with solid angle dispersion by adding orientation variability to the myocardial cells, as shown in Fig. 3(a). The orientations of the myocardial cells in each voxel are normally distributed and centered, with a standard deviation σ (solid dispersion angle) of 15°. In other words, the volume is now composed of myocardial cells that are not parallel to each other. The azimuth angle θ of the volume sample is still set to a fixed 45° and the elevation angle Φ is set to 0°.

Again from Eq. (1), we calculated the amplitude of the output light amplitude of the PLI system as a function of the rotation angle of the crossed polarizer pair, and plotted it in

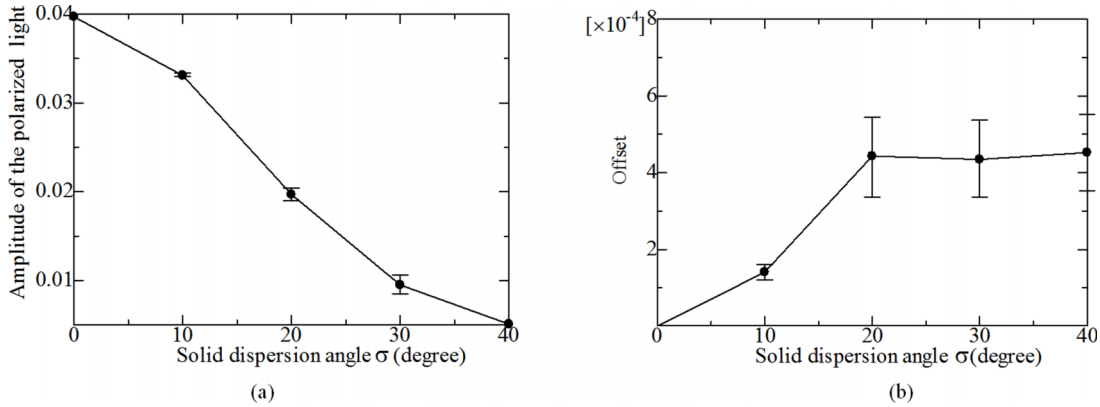

FIG. 4. Variation of the maximum amplitude of the polarized light (a) and offset (inhomogeneity level) as a function of solid angle dispersion.

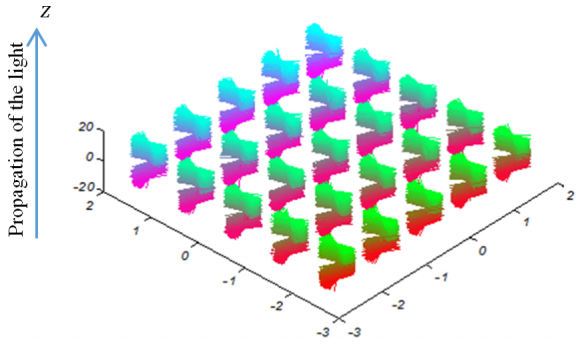

FIG. 5. Simulated volume with myocardial cell crossing.

Fig. 3. Note that the curve in Fig. 3(b), which corresponds to the solid dispersion angle 0, is the same as that in Fig. 2, which corresponds to the elevation angle 0. So, compared to the curve with the 0 solid dispersion angle, the other four curves corresponding to non-null solid dispersion angles present an offset at the rotation angle of 45°, which indicates that some inhomogeneity in orientation of the myocardial cells in the volume exists. The fact that the amplitude of the polarized light is not zero at 45° reflects the light leakage. This light leakage in the second polarizer depends on the summation of the disorders of the myocardial cells in the volume. This disorder depends on the standard deviation σ in orientation of myocardial cells. For a given rotation angle of the two crossed polarizers, when the solid dispersion angle increases, the amplitude of the output polarized light decreases.

Figure 4 shows the variations of the maximum amplitude of the output polarized light and the offset (i.e., inhomogeneity level) as a function of solid dispersion angle that varies from 0° to 40°. As observed, the solid dispersion angle can modify not only the maximum amplitude of the polarized light, but also generate offset or inhomogeneity. When the solid dispersion angle increases, the maximum amplitude of the output polarized light decreases, and the inhomogeneity level increases. But, when the solid dispersion angle attains a certain level, the inhomogeneity level changes little.

3.C. Heterogeneous volume with myocardial cell crossing

To study the variation of inhomogeneity level in the case of myocardial cell crossing, two populations of myocardial cells were simulated in the volume. The first population has a fixed azimuth angle of 0° and the second population has an azimuth angle that varies from 0° to 90°, thus creating myocardial cell crossing (Fig. 5).

As before, Eq. (1) was used to calculate the amplitude of the output polarized light for the volume formed of crossed myocardial cells. Theoretically, when the optical axes of the two populations of myocardial cells are parallel, the amplitude of the polarized light is at its maximum in the case where the selection axis of the first polarizer is at 45° from the two populations of parallel myocardial cells. Otherwise, the light amplitude begins to decrease when the myocardial cell crossing angle increased, and an offset begins to appear. In Fig. 6(a), we observe that myocardial cell crossing angle modifies strongly the amplitude of the output polarized light. Figure 6(b) shows that the azimuth angle of the volume increases when the crossing angle between myocardial cells increases. The resulting azimuth angle of the volume is the bisector of the angle formed by the two populations of myocardial cells (i.e., for each myocardial cell crossing, the azimuth angle is divided by two). Figure 6(c) represents the minimum amplitude of the output polarized light, which represents the offset of the curve with respect to the horizontal abscissa axis. We observe that the offset that represents the inhomogeneity level of myocardial cells begins to decrease from a value different from zero because the volume is not totally homogeneous and contains cell crossing.

3.D. Validation of the simulations

3.D.1. Experimental apparatus

The elements of the experimental PLI apparatus used to validate the simulations are shown in Fig. 7. The real optical elements are disposed in the same manner as in Fig. 1.

In Fig. 7, the unpolarized light source is mounted on a fixed support with the light beam directed upward to the z axis. All the optical elements are positioned along the z axis in order to be crossed by the maximum of the light. The depolarizer is placed at the output of the unpolarized light source in order to diffuse the light output homogeneously in the optical bench. Two linear polarizers are mounted on a movable carrier, and each polarizer is driven by a stepper motor. Two belts make the link between the motors and the polarizers. The first polarizer is placed above the depolarizer and set to angle α_1 equal to 0°, and the second polarizer is set near to

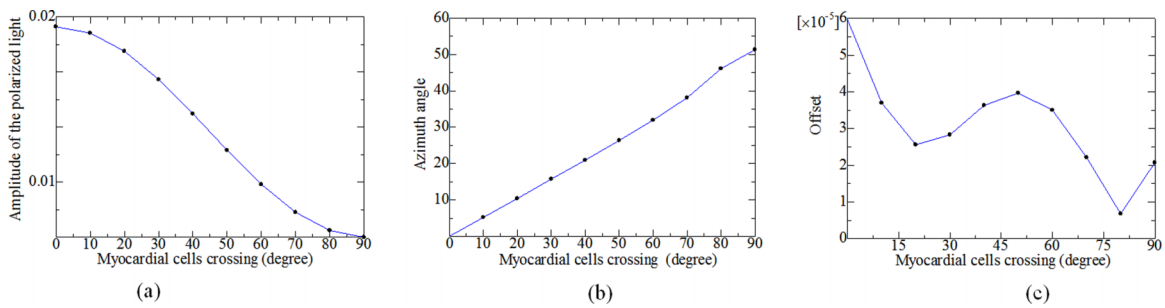

FIG. 6. Variation of the amplitude of the polarized light (a), azimuth angle (b), and offset (c) as a function of myocardial cell crossing angle.

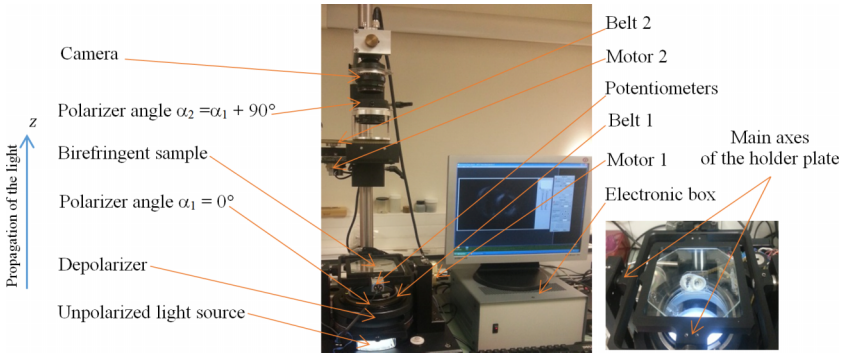

FIG. 7. The experimental PLI apparatus used to validate the simulations. On the right side is shown the zoomed version of the holder plate.

the camera with an angle equal to $\alpha_2 = \alpha_1 + 90°$. The angular position of the two polarizers can be adjusted in the system. The birefringent sample is held on a holder plate which is positioned between the two linear polarizers. The holder plate is a gyroscopic system made up of two plates (two main axes). The big plate can tilt to *Oy* axis and the small plate can tilt to *Ox* axis. The orientation of the plates helps us to control the elevation and azimuth angles of the birefringent sample in the system. The digital camera (CCD) is mounted on the top of the system to record the images. The rotation of the motors and the potentiometers are managed by an electronic box that is equipped with microcontrollers, and the communication between the electronic box and the computer is ensured via a RS232 link. Finally, we developed software codes in c/c++ to control the motor rotation, potentiometers position, and image recording.

3.D.2. Ethics statement and real tissue sample information

This study was performed on routine histological sections of hearts of human fetus and infants embedded in MMA.[11,12,16] All the tissues were obtained and processed in compliance with French legal and ethical guidelines. The investigation is conformed to the principles outlined in the declaration of Helsinki.[25,26] More precisely:

"Grenoble University Teaching Hospital owns a legally declared collection of embedded tissue sections collected

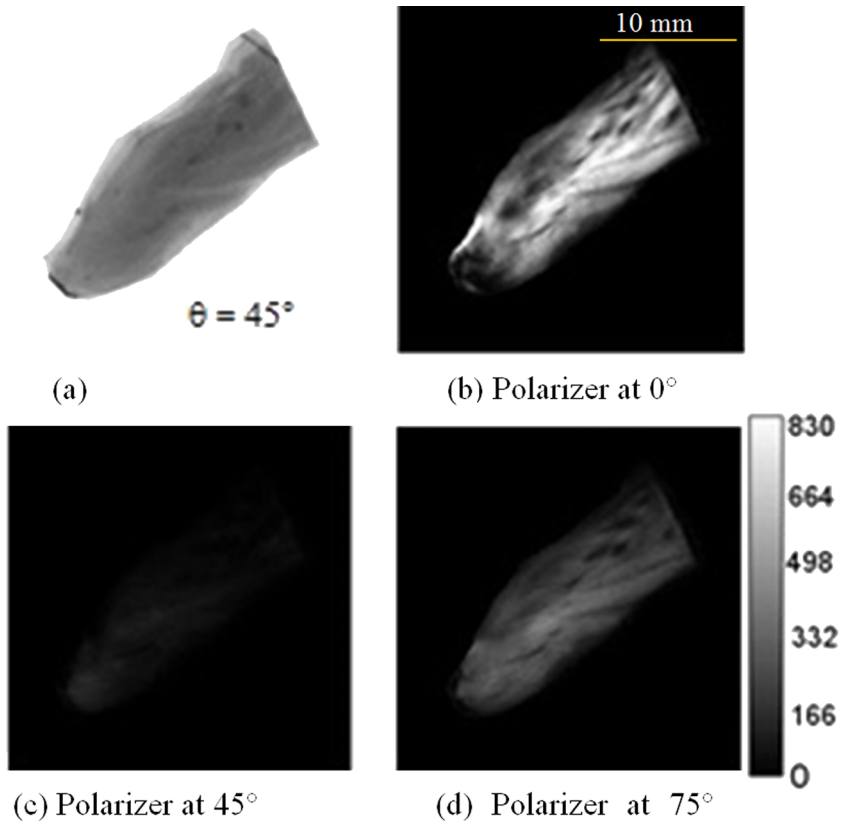

FIG. 8. Different images of the same pillar of the AVV under different polarized light imaging conditions. (a) When placed between two parallel polarizers. (b) When placed under two crossed polarizers. (c) When the selection axis of the first polarizer was set to 45°. (d) The selection axis of the first polarizer is not parallel to the optical axis of myocardial cells in the pillar of the AVV.

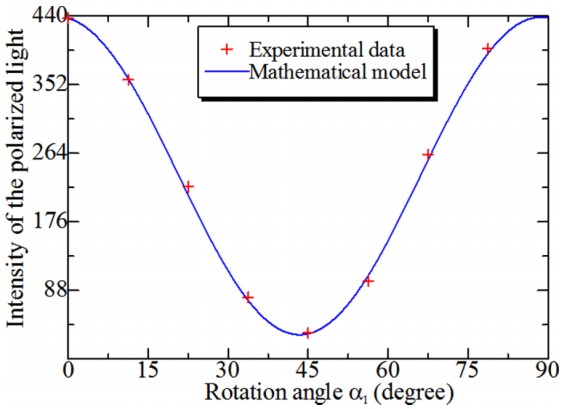

FIG. 9. Experimental data (red cross) vs mathematical model (blue color curve). The azimuth angle of the optical axis of the pillar of the AVV and the selection axis of the first polarizer were set to 45°. The amplitude of the polarized light is maximum when the selection axis of the polarizer is set to 0° while the pillar of AVV is still set to an azimuth of 45°.

after autopsy for perinatal and infant death realized for a diagnostic purpose. Written consent has been obtained from the parents/guardians at the time of the request for autopsy authorization and for research authorization on normal and abnormal development. The research protocol for this study was specifically approved by the institutional review board of the Grenoble University Teaching Hospital. Samples dedicated to research purpose were anonymized."

In order to validate the proposed PLI simulations on real tissues, we chose the pillars of the auriculo-ventricular valve

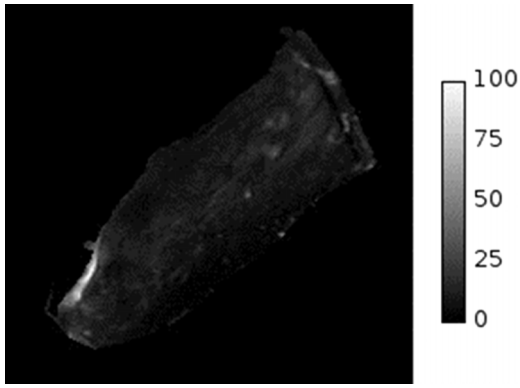

FIG. 10. Map of inhomogeneity levels of the pillar of AVV.

(AVV) of the human heart and imaged it using the experimental apparatus in Fig. 7. The AVV sample came from a fetal heart (33 amenorrhea weeks, ventricular weight 12 g, and atria weight 3 g).

The pillar of the AVV is a sort of hamstring whose role is to hold the mitral valve (left ventricle) and the tricuspid valve (right ventricle) to prevent blood from replenishing in a wrong direction. This sample was chosen for two reasons:

(a) it is anisotropic, and the orientation of its myocardial cells is well known,[14,16,23]
(b) it has a high homogeneity level in comparison with other regions of the heart. In order to explore the birefringence of the pillar of the AVV, a protocol has been

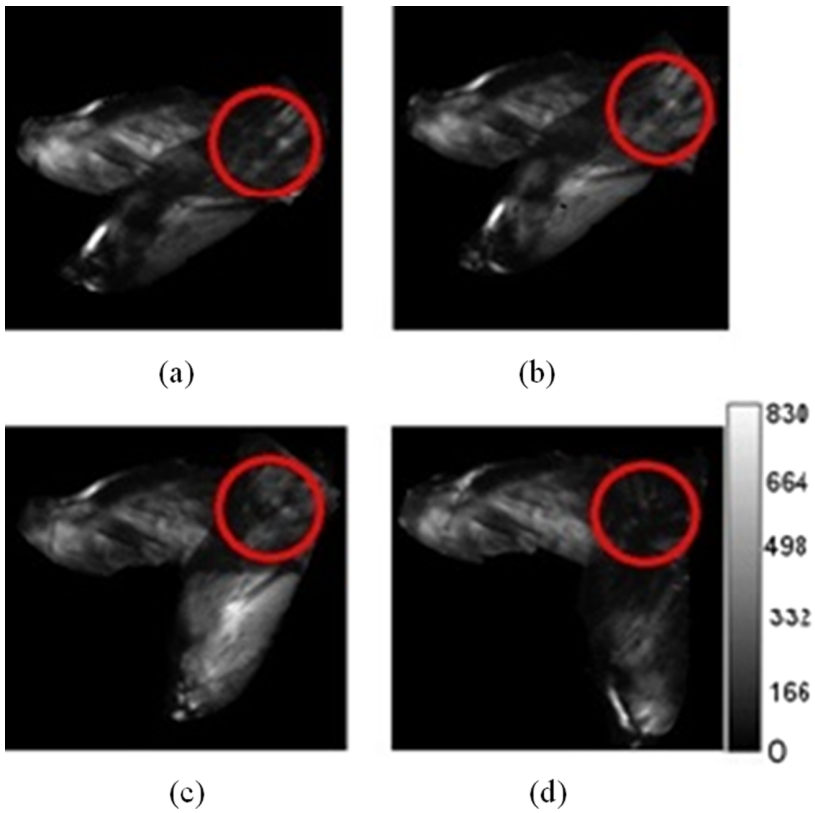

FIG. 11. Four examples of physical myocardial cell crossing obtained by superposing two pillars of the AVV. The red circle designates the ROI in which the variation of the amplitude of the polarized light is measured to calculate the inhomogeneity level map (parameter A).

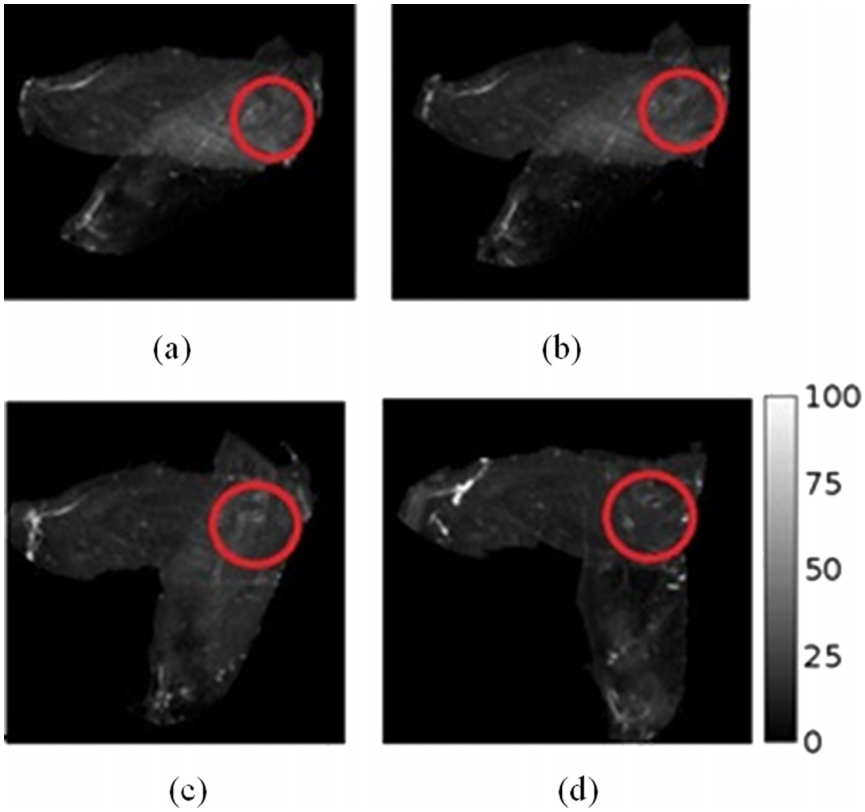

FIG. 12. Maps of inhomogeneity levels corresponding to the four myocardial cell crossing angles.

described by Jouk *et al.*[11,14,16] and more details about this tissue can be found in Refs. 11, 12, 14, and 23. To be in the same condition as that in our simulation, we have chosen two pillars of the AVV with a thickness of 250 μm. By superposing them, we obtained one pillar with thickness of 500 μm.

3.D.3. Real tissue sample preparation and recording

After removal from the thorax, the heart was perfused and fixed in a solution of 4% neutral buffered formaldehyde, and then immersed for 1 week in the same solution. The ventricles were then removed by severing the atria 1 mm proximal to the auriculo-ventricular groove and the great vessels 3 mm from the ventricle. After that, the ventricles were embedded in a resin of MMA using a protocol.[23] The specimen was infiltrated under vacuum (10 mbar) at room temperature in a series of mixtures of glycol methacrylate (GMA) and MMA in which the concentration of MMA was gradually increased to obtain pure MMA. The heart was then embedded by polymerization of MMA at 32 °C. It can be oriented according to the prerequisite referential system: coronal, transversal, or sagittal. This is done by polishing the base of the block, which is mounted on the microtome stage and determines the plane of serial sectioning: parallel to the diaphragmatic face of the heart for transversal sections; parallel to the muscular ventricular septum (VS) for sagittal sections; and parallel to the atrioventricular junctions for coronal sections. Before sectioning, three parallel holes of 1 mm diameter were drilled perpendicular to the base, to provide fiducial markers. Then, a series of thick sections (500 μm) were cut with a rotary microtome (Leica SP1600, Leica Biosystems, Wetzlar, Germany). There is a gap of 250 μm between sections due to the thickness of the saw. The rate of penetration of the saw was set to a low speed (15 min/section) in order to avoid mechanical stress and distortions.

In the present experiment, the images were recorded by setting the azimuth angle of the pillar of the AVV to 45° as in the simulation cases. The light amplitude collected by the PLI system being a function of the elevation and azimuth angles of the myocardial cells in the pillar of the AVV, it is necessary to record images at different angles. To measure the amplitude of the polarized light at each voxel, the two crossed polarizers were turned together at the same time with a step of 11.25°–78.75° with the pillar of the AVV positioned between them, generating a stack of eight images corresponding to eight angles (0°, 11.25°, 22.5°, 33.75°, 45°, 56.25°, 67.5°, 78.75°).

Figure 8(a) shows the case in which all the light is transmitted (the selection axes of the two polarizers were parallel). In Figs. 8(b)–8(d), we show three images corresponding to three angles (0°, 45°, 78°) for illustration. In Fig. 8(b), the selection axis of the first polarizer was set to 0° and that of the second polarizer to 90°(crossed polarizers). The amplitude of the polarized light is maximum in this case, since the optical axis of the pillar of the AVV was set to 45°. We should keep in mind that, to avoid losing the reference of measurements, the selection axes of the two polarizers must be perpendicular to each other (forming a crossed polarizers) during image recording. In Fig. 8(c), the selection axis of the first polarizer was set to 45°. In principle, all the light amplitude must be

TABLE I. Physical measurements of inhomogeneity levels as a function of myocardial cell crossing angles.

Myocardial cells crossing angles (deg)	30	45	60	90
Inhomogeneity levels	24.2	13.3	18.8	10.7
Output polarized light	227.5	201.4	74.0	24.2
Azimuth angles	15.4	21.1	32.0	46.8

zero according to the simulation results. In practice, the light amplitude is not equal to zero and instead it is attenuated according to the simulation results on heterogeneous volumes. We observe that many regions of the pillar of the AVV are totally dark, implying that the optical axes of those myocardial cells are parallel to the selection axis of the first polarizer (as observed in the simulations). The regions that are not totally dark indicate that all the myocardial cells are not parallel to the selection axis of the first polarizer. In Fig. 8(d), the light intensity begins to increase since the selection axis of the first polarizer is not parallel to the optical axis of myocardial cells in the pillar of the AVV.

3.D.4. Inhomogeneity level of simple pillars of AVV

As in the simulated tissue case, we first measure the variation of the amplitude of the polarized light as a function of the rotation angle of the two polarizers with various solid dispersion angles. Figure 9 shows the theoretical result (blue color curve) and real result (red cross data points) from the pillar of the AVV in a voxel. We found exactly the same results as those in simulations. When the selection axis of the first polarizer was set to 0°, i.e., the rotation angle $\alpha_1 = 0$, the light amplitude was maximum ($B = 437$ arbitrary unit—a.u.). Therefore, when the rotation angle of the first polarizer is parallel to the optical axis of the pillar of the AVV ($\alpha_1 = 45°$), the amplitude of the polarized light reaches its minimum (offset).[17] We also observe that the pillar of the AVV has an inhomogeneity level that differs from zero, since the light intensity curve does not reach the abscissa axis at the 45° rotation angle point. For an azimuth angle of 45°, the final amplitude $y(\alpha)$ of the polarized light depends only on the rotation angle α of the two polarizers and the value B in Eq. (8). If the pillar of AVV were totally homogeneous, the value of A in Eq. (8) would drop to zero like a totally homogeneous uniaxial birefringent crystal. In other words, the value of the offset A is dependent on the inhomogeneity level of the pillar of the AVV. A low value of the offset indicates that the sample has a low inhomogeneity level (or high homogeneity level). By fitting the analytical model Eq. (8) to the experimental data (stack of eight images), we obtained the amplitude of the output polarized light, $B = 437$ (a.u.) and the inhomogeneity level $A = 32$ (a.u.).

Now, by fitting the analytical model Eq. (8) to the experimental data (stack of eight images) pixel by pixel, we can obtain the map of inhomogeneity levels (parameter A), as shown in Fig. 10. The dark regions indicate a low parameter A values close to zero, meaning that these regions are almost perfectly homogeneous. The brighter regions represent heterogeneous regions having greater inhomogeneity level values. If the pillar of AVV were totally homogeneous, the image in Fig. 10 would be completely dark.

3.D.5. Inhomogeneity level of crossed pillars

In the simulation cases, we have found that when myocardial cell crossing angle increased, the amplitude of the polarized light decreased. To evaluate these simulation results, we now use real data from two pillars of the AVV, both of which have a thickness of 250 μm. By superposing the two pillars with some angles, we obtain myocardial cell crossing in a region having a thickness of 500 μm (Fig. 11, red circle). In this experiment, the optical axis of the first pillar of the AVV was fixed to an azimuth angle of 0° relative to the selection axis of the first polarizer, and the second pillar was rotated to generate specific myocardial cell crossing.

Figure 11 shows four images corresponding to four myocardial cell crossing angles of 30°, 45°, 60°, and 90°, respectively. All the maps in Fig. 11 have been scaled into the same grey level dynamic range for measurements. The red circle indicates the region of interest (ROI) for the measurement.

For each crossing angle, a stack of eight images was acquired. Then, Eq. (8) was used to calculate the map of inhomogeneity levels (Fig. 12). Table I gives the obtained inhomogeneity level values for different myocardial cell crossing angles. For comparison with the simulations, we also plot in Fig. 13 the three parameters as a function of myocardial cell crossing angles, as those in Fig. 6. As can be observed, the amplitude of the polarized light decreases with the myocardial cell crossing angle, the azimuth angle is the bisector of the angle formed by the two crossed pillars of the AVV, and the inhomogeneity level decreases from an initial value different from zero (because the pillar of AVV was not totally homogeneous) as those in Fig. 6.

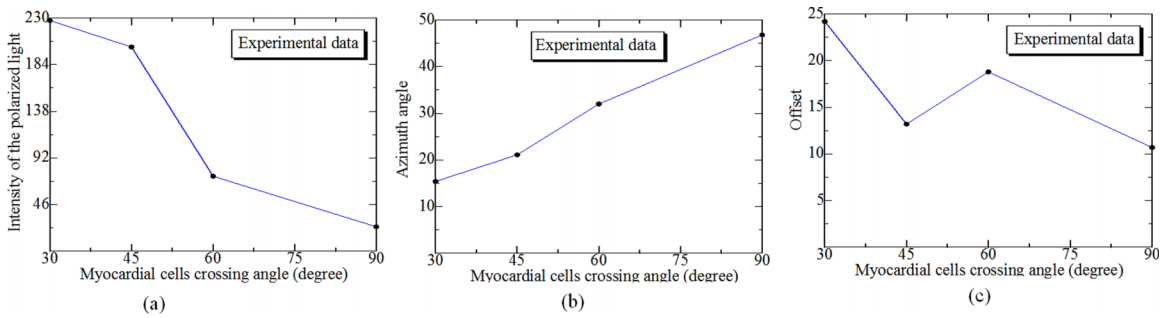

FIG. 13. Physical measurements of the variation of the polarized light amplitude (a), azimuth angle (b), and inhomogeneity level (c).

4. CONCLUSION

We have proposed a PLI simulation method to study the optical properties of myocardial cells in the human heart. To our knowledge, this is the first study that has enabled the quantitative description of the spatial arrangement of myocardial cells in the human heart using PLI. The results on both simulated and real tissues showed that the proposed method enables physical information, such as the myocardial cell inhomogeneity level, polarized light intensity, and myocardial cell azimuth angle, of myocardial tissues to be estimated, and that the inhomogeneity level of a volume or voxel, which depends strongly on the spatial arrangement of myocardial cells, can be quantified, which opens new ways to study the microstructures of the human myocardium.

ACKNOWLEDGMENT

This work was supported by the French ANR under MOSIFAH ANR-13-MONU-0009-01.

[a]Author to whom correspondence should be addressed. Electronic mail: desrpaaud@gmail.com

[1]C. C. Fox and G. M. Hutchins, "The architecture of the human ventricular myocardium," Johns Hopkins Med J. **130**(5), 289–299 (1972).
[2]D. D. Streeter, Jr., "Gross morphology and geometry of the heart," in *Handbook of Physiology, Section 2* (Williams and Wilkins, American Physiological Society, Baltimore, MD, 1979), Vol. 1, pp. 61–112.
[3]F. Torrent-Guasp, "The cardiac muscle," *Fundacion Juan March*, 15-134 (Madrid, 1973).
[4]R. A. Greenbaum, S. Y. Ho, D. G. Gibson, A. E. Becker, and R. H. Anderson, "Left ventricular fibre architecture in man," Br. Heart J. **45**, 248–263 (1981).
[5]W. Hort, "Makroskopische und mikrometrishe untersuchungen am myokard verschieden stark gefüllter linker kammeen," Virchows Arch. Pathol. Anat. Physiol. **333**(6), 523–564 (1960).
[6]P. Basser and C. Pierpaoli, "Microstructural and physiological features of tissues elucidated by quantitative-diffusion-tensor MRI," J. Magn. Reson. Imaging **111**(3), 209–219 (1996).
[7]M. T. Wu, W. Y. Tseng, M. Y. Su, C. P. Liu, K. R. Chiou, V. J. Wedeen, T. G. Reese, and C. F. Yang, "Diffusion tensor magnetic resonance imaging mapping the fiber architecture remodeling in human myocardium after infarction," Circulation **114**(10), 1036–1045 (2006).
[8]C. Frindel, M. Robini, J. Schaerer, P. Croisille, and Y. M. Zhu, "A graph-based approach for automatic cardiac tractography," Magn. Reson. Med. **64**, 1215–1229 (2010).
[9]P. Scmid, T. Jaermann, P. Boesiger, P. F. Niederer, P. P. Lunkenheimer, C. W. Cryer, and R. H. Anderson, "Ventricular myocardial architecture as visualized in postmortem swine hearts using magnetic resonance diffusion tensor imaging," Eur. J. Cardio-Thorac. Surg. **27**, 468–472 (2005).
[10]P. Whittaker, D. R. Boughner, and R. A. Kloner, "Analysis of healing after myocardial infarction using polarized light microscopy," Am J Pathol. **134**(4), 879–893 (1989).
[11]P.-S. Jouk, Y. Usson, G. Michalowicz, and L. Grossi, "Three dimensional cartography of the pattern of the myofibres in the second trimester fetal human heart," Anat. Embriol. **202**, 103–118 (2000).
[12]P.-S. Jouk, A. Mourad, V. Misilic, G. Michalowicz, A. Raoul, D. Caillerie, and Y. Usson, "Analysis of the fiber architecture of the heart by quantitative polarized light microscopy. Accurancy, limitations and contribution to the study of the fiber architecture of the ventricles during fetal and neonatal life," Eur. J. Cardio-Thorac. Surg. **31**(5), 915–921 (2007).
[13]J. Rieppo, J. Hallikainen, J. S. Jurverlin, I. Kiviranta, J. Heikki Helminen, and M. M. Hyttinen, "Practical considerations in use of polarized light microscopy in the analysis of the collage network in cartilage," Microsc. Res. Tech. **71**, 279–287 (2008).
[14]P.-S. Jouk, "Etude de la topographie des cellules myocardiques au cours du développement embryonnaire et fœtal," Ph.D. thesis, GRENOBLE-BU Sciences, 1994.
[15]M. F. Wood, N. Ghosh, M. A. Wallenburg, S. H. Li, R. D. Weisel, B. C. Wilson, R. K. Li, and I. A. Vitkin, "Polarization birefringence measurement for characterizing the myocardium, including healthy, infarcted, and stemcell-regeneration tissues," J. Biomed. Opt. **15**(4), 047009 (9pp.) (2010).
[16]Y. Usson, F. Parazza, P.-S. Jouk, and G. Michalowicz, "Method for the study of the three dimensional orientation of the nuclei of myocardial cells in fetal human heart by means confocal scanning laser microscopy," J. Microsc. **174**(2), 101–110 (1994).
[17]P. A. Desrosiers, G. Michalowicz, P.-S. Jouk, Y. Usson, and Y. Zhu, "Modeling of the optical behavior of myocardial fibers in polarized light imaging," in *MICCAI STACOM*, 2012.
[18]M. Wolfman, "Polarized light microscopy as a tool of diagnostic pathology," J. Histochem. Cytochem. **23**, 21–50 (1975).
[19]D. L. Taylor, "Birefringence changes in vertebrates striates muscle," J. Supramol. Struct. **3**, 181–191 (1975).
[20]W. C. McCrone, B. L. McCrone, and J. G. Delly, *Polarized Light Microscopy* (Research Institute, Chicago, IL, 1984).
[21]W. R. Phillips, "Mineral optics, principles and techniques," in *International Standard Book* (W. H. Freeman and Company, San Francisco, CA, 1977).
[22]F. Brehat and B. Wyncke, "Représentation des états de polarisation des ondes lumineuses" (2003).
[23]P.-S. Jouk, Y. Usson, G. Michalowicz, and F. Parazza, "Mapping of the orientation of myocardial cells by means of polarized light and confocal scanning laser microscopy," Microsc. Res. Tech. **30**(6), 480–490 (1995).
[24]R. H. Anderson and A. E. Becker, "An integrated text color atlas," in *Cardiac Anatomy* (Grower Medical Publishing, Churchill Livingstone, Edinburgh-London, 1983).
[25]http://www.wma.net/fr/30publications/10policies/b3/.
[26]R. V. Carlson, K. M. Boyd, and D. J. Webb, "The revision of the declaration of Helsinki: Past, present and future," Br. J. Clin. Pharmacol. **57**(6), 695–713 (2004).